

Water Resources Research[®]

RESEARCH ARTICLE

10.1029/2021WR030380

Special Section:

Advancing process representation in hydrologic models: Integrating new concepts, knowledge, and data

Key Points:

- Vegetation-generated turbulent kinetic energy has considerable impact on the sediment deposition probability in vegetated channels
- Turbulence dominates sediment deposition and resuspension motions when the dimensionless turbulent kinetic energy is larger than the threshold
- Random displacement model simulates the sediment net deposition in vegetated channel flows with the deposition and resuspension model

Correspondence to:


W. Huai,
wxhuai@whu.edu.cn

Citation:

Yang, L., Huai, W., & Guo, Y. (2021). Stochastic simulation of the suspended sediment deposition in the channel with vegetation and its relevance to turbulent kinetic energy. *Water Resources Research*, 57, e2021WR030380. <https://doi.org/10.1029/2021WR030380>

Received 11 MAY 2021
Accepted 26 AUG 2021

Stochastic Simulation of the Suspended Sediment Deposition in the Channel With Vegetation and Its Relevance to Turbulent Kinetic Energy

Liu Yang¹ , Wenxin Huai¹ , and Yakun Guo² 

¹State Key Laboratory of Water Resources and Hydropower Engineering Science, Wuhan University, Wuhan, China,

²Faculty of Engineering & Informatics, University of Bradford, Bradford, UK

Abstract The aquatic vegetation patch plays a significant role on sediment net deposition in the vegetated channels. Particularly, the flow is decelerated at the leading edge of a patch that tends to induce vertical updraft, that is, a diverging flow region, in which vegetation greatly affects the pattern of sediment net deposition. This study focuses on the simulation of the sediment net deposition in the whole vegetation patch region through an innovative random displacement model, a Lagrange method, with probability-based boundary conditions, instead of the reflection or sorption boundary at the channel bottom. The probability model of deposition and resuspension is proposed according to the flow field characteristics in the different regions of the vegetation patch. The variation of the sediment deposition and resuspension with the turbulent kinetic energy is analyzed to illustrate the effect of the turbulence induced by vegetation, represented by the dimensionless turbulent kinetic energy (ψ), on the sediment deposition and resuspension. The sediment deposition predicted by the proposed model agrees well with the experimental measurements. Results show that the effect of vegetation on the sediment deposition and resuspension motions begins to prevail when the vegetation-induced ψ is larger than its threshold, ψ_* . The threshold of ψ is predicted to be within 6.8–10 according to the simulation results in this study. As the turbulent kinetic energy increases, the deposition probability decreases continuously when $\psi > \psi_*$.

1. Introduction

The turbulent vortices in the vegetated open channel flow are mainly generated by the vegetation and are remarkably larger than the vortices induced by the bed shear stress in the channel without vegetation (Ghisalberti & Nepf, 2004). Aquatic vegetation also plays an important role in the suspended sediment transport (Huai et al., 2020), bed-load sediment transport (Yang & Nepf, 2018), and sediment deposition and bedform (Yang & Nepf, 2019). Sediment deposition in the vegetated channel flows is receiving considerable attention in recent decades (Beuselinck et al., 2000; Follett & Nepf, 2018; Kim et al., 2018; Mark et al., 1983). There are two opposite effects of the aquatic vegetation on sedimentation. Aquatic vegetation usually enhances the sediment deposition and produce a region of sediment retention; while they also generate additional drag and obstruction which restrains flow velocity and reduces the sediment carrying capacity (Abt et al., 1994; Gacia et al., 2003; Zhang et al., 2020; Zong & Nepf, 2010). However, some researchers also observed that the reduction of deposition occurred in the vegetation region as many vortices were generated by the vegetation stems comparing with the flow in the bare-bed channel (Follett & Nepf, 2012; Ganthy et al., 2015; Lawson et al., 2012). Improvement of the sediment management in natural rivers, such as sediment retention and erosion in the vegetation region, is important for river management. As such, understanding the impact of the aquatic vegetation on the sediment deposition and resuspension is essential to predict retention or erosion.

Extensive studies have been conducted using various methods to investigate the impact of the aquatic vegetation on the sediment deposition (Huai et al., 2021). Among these studies, laboratory experiment is the most widely used method to investigate the sediment deposition in the vegetated channel flows. Follett and Nepf (2018) conducted experiments to study the retention of the graded sediment particles in a submerged meadow. They found that both the position of particles released and the particle size affected the pattern of sediment retention. Zhang et al. (2020) and Zong and Nepf (2010) also studied the sediment deposition in the channel with vegetation through laboratory flume experiments. Zhang et al. (2020) focused on

investigating the effect of the submerged vegetation density and flow velocity on the deposition pattern, while Zong and Nepf (2010) described the effect of the emergent vegetation on the sediment deposition. Though it is convenient and direct to obtain the pattern of the sediment deposition in the vegetation patch using the laboratory flume experiment, its inefficiency and scale effect restrain the development of studies. With the development of computing resources and computational fluid dynamics techniques, numerical models have also been widely developed and applied to simulate various turbulent flows. However, to the authors' best knowledge, numerical studies on the sediment deposition in the vegetation patch are still limited (Kim et al., 2018; Tsujimoto, 1999). These two studies developed a depth-averaging two-dimensional (2-D) model to analyze the profile pattern of the sediment deposition in the vegetation region. However, the depth-averaging model is only suitable for shallow water in a relatively wide channel, while many vegetated channel flows are not shallow water flow. As such, the present study attempts to explore the application of the random displacement model (RDM) to investigate the sediment deposition in the channel with the vegetation patch, not just in the shallow water channels. The RDM, which is a Lagrange method, was developed to study the profile of the suspended sediment concentration in the channels with vegetation by the authors (Huai, Yang, et al., 2019) who expanded the model to study the suspended sediment transport in the vegetated channel flows; and Follett et al. (2019) studied the retention of pollen in the flow with different released height of particles through RDM. This study will further explore the application of the RDM to the sediment deposition pattern in the vegetated sediment-laden flows.

Two sediment movement processes, that is, the deposition and the resuspension, are introduced to explore the pattern of the sediment net deposition in the channel with vegetation. Resuspension will occur if the instantaneous velocity near the channel bed is larger than the critical velocity of the sediment incipient motion. Obviously, the net deposition is reduced with the increase of the sediment resuspension. The models involved in the sediment incipient motion are usually based on the bed shear stress τ , such as the most prevalent Shields number θ (Beheshti & Ataie-Ashtiani, 2008; Guo, 2020; Tinoco & Coco, 2016), which is the most representative achievement and is still widely used. However, the stress model has been shown to be inaccurate in terms of the channel with bedforms and vegetation (Nelson et al., 1995; Yager & Schmeeckle, 2013). Some recent studies show that it is the turbulence rather than the bed shear stress which dominates the sediment transport (Houssais et al., 2015) and this situation is more evident in the vegetated channel flows. In the bare-bed channel, the turbulent kinetic energy linearly relates to the bed shear stress (Stapleton & Huntley, 1995), while the turbulent kinetic energy in the vegetated channel flows is primarily generated by the aquatic vegetation (Tanino & Nepf, 2008) and causes τ being no longer a substitute for turbulence. Thus, the turbulent kinetic energy model is widely used to simulate the onset motion of the sediment in the vegetation channel flows in recent decades (Tang et al., 2019; Tinoco & Coco, 2018; Yang & Nepf, 2019; Yang et al., 2016; Zhang et al., 2020). Yang et al. (2016) predicted the turbulent kinetic energy k in the vegetated channels from a depth-averaged velocity U and vegetation density, that is, volume fraction ϕ . Their results demonstrated that the application of the turbulent kinetic energy provided a good prediction of the bed-load transport rate. Tinoco and Coco (2018) focused on investigating the relationship between the turbulent kinetic energy and resuspension using the laboratory experiments. They emphasized that the turbulent kinetic energy induced by the flow-vegetation interactions, rather than bed shear stress by mean velocity, was the main driver of the resuspension within the array. Previous studies have only focused on the expression of the turbulent kinetic energy and the relationship between the turbulent kinetic energy and the resuspension or the bed-load transport rate. However, studies about the turbulent kinetic energy and the deposition probability are still rare, which motivates the present study.

This study aims at improving the turbulent kinetic energy model to simulate the sediment deposition and the resuspension in the vegetated channel flows through an innovative RDM. The main contributions of this study include several aspects. First, this study applies the RDM to investigate the sediment deposition, thereby extending the application of the model and providing a new research methodology for the sediment deposition. Second, we propose a deposition and resuspension probability model based on the previous turbulent kinetic energy models. The probability of the sediment deposition and resuspension varies from the leading edge of the vegetation patch to the end of the patch according to the flow field features in the different vegetation patch regions. Third, the results of the present study demonstrate that the aquatic vegetation dominates the sediment deposition when the value of the dimensionless turbulent kinetic energy is larger than the proposed threshold ψ_c . The model is validated with the net deposition measured in the

laboratory flume, showing the accuracy of the proposed model in predicting the sediment net deposition in the vegetated channels.

2. Methods

2.1. Numerical Model

Since Taylor's (1921) pioneered work on the turbulent dispersion of a passive tracer using the Lagrangian approach, the RDM, which is a trajectory model, has been used in studying particles trajectory in the turbulent atmospheric flows. Wilson (2000) provided the source and concept of the RDM. In this study, the RDM is applied to trace the particles in the open channel flows with the aquatic vegetation. Recently, Huai, Yang, et al. (2019) applied the RDM to simulate the suspended sediment concentration in the vegetated channel flows. This study tracks the motion of sediment particles in the vegetated channels with the sediment deposition being innovatively considered at the bottom of the channel. Though details of the RDM can be found in Huai, Yang, et al. (2019), we provide a brief conception of the RDM for convenience and completeness.

For the vertical 2-D simulation, the displacement of sediment particles is modeled as follows:

$$\Delta x = u(z) \cdot \Delta t, \quad (1)$$

$$\Delta z = \left(\frac{dK_z(z)}{dz} - \omega \right) \cdot \Delta t + w\Delta t + R\sqrt{2K_z(z)\Delta t}, \quad (2)$$

where x and z [L] are the longitudinal and the vertical coordinates, respectively; Δx and Δz [L] are the displacements of the sediment particles in the longitudinal and the vertical directions, respectively; Δt [T] is the time step; K_z [L^2T^{-1}] is the turbulent diffusion coefficient that expresses the strength of the turbulent vortex; w and u [LT^{-1}] is the vertical and longitudinal flow velocity, respectively; R [-] is a normally distributed random number with mean 0 and standard derivation 1; and ω [LT^{-1}] is the settling velocity of the sediment particles, which is estimated from Equation 4 in Cheng (1997).

The option of the boundary condition is significant for the accuracy of the RDM. The water surface is set as the reflection boundary (Huai, Yang, et al., 2019; Liu et al., 2018). However, to accurately simulate the sediment deposition, the reflection boundary is unsuitable for the bottom bed of the channel. This is considerably different from settings in previous studies.

In the present vertical 2-D model, the advection-diffusion equation of the sediment is:

$$\frac{\partial C}{\partial t} + \frac{\partial(uC)}{\partial x} + \frac{\partial(wC)}{\partial z} - \frac{\partial}{\partial x} \left(K_x \frac{\partial C}{\partial x} \right) - \frac{\partial}{\partial z} \left(K_z \frac{\partial C}{\partial z} \right) - \frac{\partial(\omega C)}{\partial z} + S = 0, \quad (3)$$

where t [T] is the time; K_x is the longitudinal dispersion coefficient; C [ML^{-2}] is the time-spatial averaging suspended sediment concentration and S [$ML^{-2}T^{-1}$] represents the source term. In Equation 3, the longitudinal dispersion term could be ignored because the magnitudes of the term are considerably smaller than the longitudinal advection term. The sixth term in the left-hand side of Equation 3 represents the settling term, which highlights the difference between the sediment particles and pollutants (whose settling velocity is usually ignored).

The initial and boundary conditions are as follows:

$$C(0, x, z) = C_0 \phi_0(z) \delta(x), \quad (4)$$

$$K_z \frac{\partial C(t, x, 0)}{\partial z} = -\eta C(t, x, 0), \quad (5)$$

$$\frac{dC(t, x, H)}{dz} = 0, \quad (6)$$

where C_0 is the initial sediment concentration; $\phi_0(z)$ is the initial distribution function of the sediment particles in the vertical direction (uniform distribution is used in this model); $\delta(x)$ is the Dirac delta function, which means that all sediment particles are released at $x = 0$; H [L] is the flow depth; and η [LT^{-1}] is the sediment deposition rate at the bottom of the channel. Equation 5 considers the deposition boundary condition at the channel bed by introducing the parameter η , which expresses the comprehensive influence,

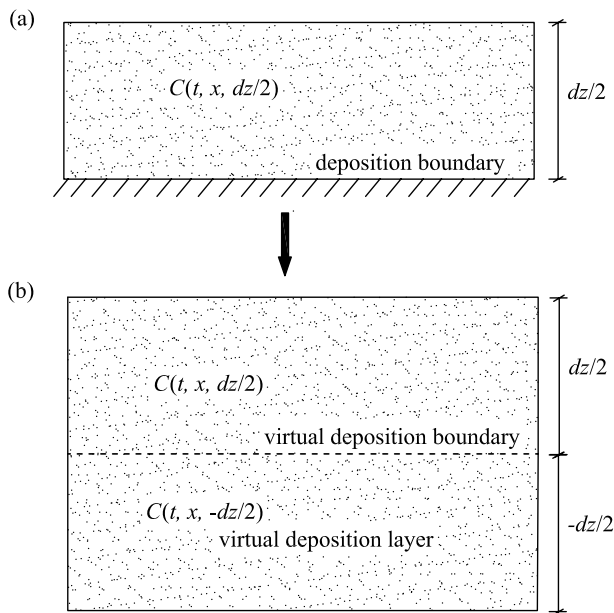


Figure 1. Conception of the sediment particle deposition probability. In (a), the sediment particles cannot pass through the boundary and deposit at the boundary according to the deposition probability. In (b), the particles can go through the virtual deposition boundary by controlling the sediment concentration consistent with Equation 8, where the same effects with (a) can be obtained.

including settling velocity and flow field, on the sediment deposition. In terms of Equation 6, the reflection boundary condition is specified at the water surface.

The bottom boundary condition can be rewritten as:

$$\frac{\partial C(t, x, 0)}{\partial z} = -\frac{\eta}{K_z} C(t, x, 0). \quad (7)$$

To understand the conception of the boundary condition at the channel bottom, the deposition boundary can be removed if the sediment concentration near the river bed satisfies the following:

$$\frac{C(t, x, dz/2) - C(t, x, -dz/2)}{C(t, x, dz/2)} \approx \frac{dC(t, x, 0)}{C(t, x, 0)} = -\frac{\eta}{K_z} dz. \quad (8)$$

Equation 8 is the finite-differential form of the concentration gradient at $z = 0$ when dz approximates to zero. The conception diagram for the deposition probability is shown in Figure 1 with a virtual deposition layer. The real channel bottom can be replaced by a virtual deposition boundary by adjusting the sediment concentration to meet the requirement of Equation 8. From this assumption, the sediment particles can pass through the virtual boundary and enter into the virtual deposition layer, where the sediment particles are supposed to be deposited, that is, the bed load.

As the value of dz in Equation 8 is negative, the deposition probability of a particle at the bottom of the channel can be expressed as:

$$P_d = \frac{C(t, x, dz/2) - C(t, x, -dz/2)}{C(t, x, dz/2)} = \left| \frac{-\eta}{K_z} dz \right|, \quad (9)$$

where $P_d [-]$ is the deposition probability of the sediment particles expressing the comprehensive effects of vegetation on flow field and can be obtained from the numerical simulation.

2.2. Flow Field Domain

Aquatic vegetation patch, acting as a barrier, considerably alters the flow field structure, as shown in Figure 2. In submerged vegetated channel flows, the flow velocity is decelerated when water flow enters into the submerged vegetation patch. Meanwhile, the flow deceleration triggers a vertical updraft where the vertical velocity w sharply increases. This flow adjustment begins at the entrance edge of the vegetation patch and develops along the permeating the vegetation region. This flow adjustment then completes at the

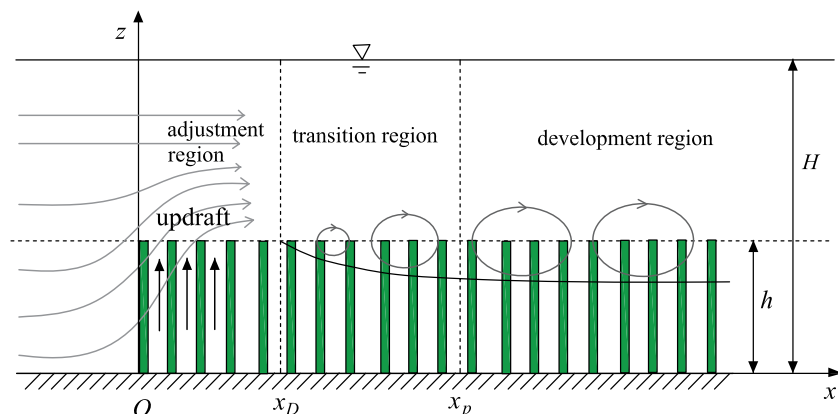


Figure 2. Sketch of the flow field structure in the vegetation patch. The flow field is divided into three regions according to the flow features: adjustment, transition, and development regions.

position $x = x_D$, where the updraft approximates to vanish. According to the study of Chen et al. (2013), the adjustment length x_D [L] is a function of the vegetation density, the flow depth, and the drag coefficient:

$$x_D = (6.9 \pm 1.1)(1 - \phi)h + \frac{3.0 \pm 0.4}{C_D a}(1 - \phi), \quad (10)$$

where ϕ [-] is the solid volume fraction within the vegetation region, a [L^{-1}] is the front area of vegetation per volume, h [L] is the height of vegetation, and C_D [-] is the drag coefficient induced by vegetation.

Velocity decreases suddenly near the top of the vegetation due to the barrier effect induced by the vegetation on the velocity within the patch region. At the same time, overflow is accelerated. Therefore, a shear layer with coherent vortex structure begins to develop within the adjustment region. The development of the shear vortex is constrained within the adjustment region by the vertical updraft (Ghisalberti, 2002; Raupach et al., 1996). For this reason, the shear vortex, that is, the mixing layer, begins to develop at the end of the adjustment region x_D and reaches the highest scale of vortex at $x = x_p$, as shown in Figure 2. Downstream the position x_p , the flow structure reaches a developed state. The length of x_p depends on the scale of the vortex structure and is determined by the vegetation density and the depth of submergence (Chen et al., 2013). Details on determining the value of x_p can be found in Chen et al. (2013).

The discussion above demonstrates the complexity of flow field structure in the channel with vegetation. According to the governing equation of the RDM, that is, Equations 1 and 2, the flow field parameters, namely the flow velocity and turbulent diffusion coefficient, are vital for the particles motion. To obtain the complex flow field parameters, in present study, realizable k - ϵ turbulence model and porous model are used to simulate the flow field in vegetated channels. The vegetation region is simulated as a porous zone by adding drag force terms to the momentum equations. The drag force term exerted by vegetation can be modeled as:

$$f_i = \frac{1}{2} \frac{C_D a}{1 - \phi} \bar{u}_i \sqrt{\bar{u}_j \bar{u}_j}. \quad (11)$$

where f_i is the vegetation-induced drag in the x_i direction; \bar{u}_i is the temporal averaged velocity component in the x_i direction. More information about the porous model and coefficient C_D can be found in Ai et al. (2020).

As for the turbulent diffusion coefficient, it is very complicated in the channel with submerged vegetation. In the present study, to simplify the model, the turbulent diffusion coefficient is approximated as the same as the profile of Huai, Yang, et al. (2019) in the transition and developed regions. They determined the turbulent diffusion coefficient in several typical positions, that is, top of vegetation (Ghisalberti & Nepf, 2005) and wake region in the vegetation zone (Nepf et al., 2007), according to the previous experimental research outcomes; and then linearly connected several positions. This turbulent diffusion coefficient model has been used and verified by many researchers (Follett et al., 2016; Huai, Yang, et al., 2019). In the adjustment region, the vertical flow velocity dominates the vertical mass transport as the effect of updraft is larger than diffusion. In the present model, it is reasonable to ignore the vertical turbulent diffusion term in this region, which could also be verified from the agreement between simulated sediment deposition and experiment measurements deposition.

It is important to note that the flow velocity u and w in the submerged vegetated channel flows are simulated with the above porous and turbulence models; however, flow velocity and turbulence diffusivity in the channel with emergent vegetation are not simulated with the model. Previous researchers showed that the longitudinal velocity (Huai et al., 2009) and turbulent diffusion coefficient (Nepf, 2012) were nearly a constant in the channel with emergent vegetation; and the vertical velocity was around zero even though in the leading region of vegetation. Therefore, in the present study, the measured value is approximately used in whole flow field domain in the channel with emergent vegetation.

2.3. Deposition and Resuspension Probabilities

Gacia et al. (2003) and Zhang et al. (2020) showed that the vegetation sometimes enhances the sediment deposition in channel with submerged meadows. However, some studies illustrated that the vegetation contributed to erosion and weakened the deposition in the leading of circular emergent patch comparing with the bare bed flows (Follett & Nepf, 2012). The profile of sediment particles in the channel bed is closely

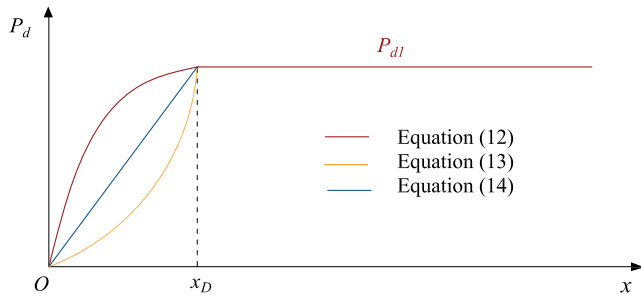


Figure 3. Diagram of three hypothetical profiles of sediment deposition probability.

associated with the amount of the deposition and resuspension. In the present study, the effect of flow field on the deposition and the resuspension is represented by the probability of the deposition and resuspension in different regions of vegetation. Although the probability boundary has been applied in the previous study (e.g., Bohrer et al., 2008), in this study, the authors propose the probability model of the sediment deposition and the resuspension according to the flow field structure in the vegetation patch.

2.3.1. Deposition Probability

The deposition of the sediment particles is affected by the flow field in the vegetated channel flows. The characteristics of the flow field vary considerably at different regions of vegetation. Because the effect of updraft on the deposition decreases along the distance to the patch entrance, we

assume that the deposition probability increases gradually from zero at the leading edge of vegetation; and the deposition probability is assumed as a constant beyond the adjustment region because the updraft disappears gradually with the shear vortex development. Three different expressions of the deposition in the adjustment region, that is, $x < x_D$, are then assumed as follows:

$$P_d = -\frac{P_{d1}}{x_D^2}x^2 + \frac{2P_{d1}}{x_D}x, \quad (12)$$

$$P_d = \frac{P_{d1}}{x_D^2}x^2, \quad (13)$$

$$P_d = \frac{P_{d1}}{x_D}x, \quad (14)$$

where P_{d1} [-] is the deposition probability outside the adjustment region. Figure 3 illustrates these hypothetical probability profiles. In this model, P_{d1} is the only unknown parameter, which will be determined according to the consistency between the simulated and measured net deposition. The best suitable expression of the deposition probability in the adjustment region will be validated in the later section by comparing observed sediment net deposition and simulated net deposition with Equations 12–14.

2.3.2. Resuspension Probability

Yang et al. (2016) derived the critical velocity of the incipient sediment motion from the turbulent kinetic energy. In the bare bed flow, the incipient sediment motion mostly depends on the bed shear stress; therefore, the critical velocity is historically related to the bed shear stress (Houssais et al., 2015; Recking, 2009), for example, critical Shields number θ_c [-]. Stapleton and Huntley (1995) showed that the role of turbulence was inherently represented in the Shields diagram because the turbulent kinetic energy and the shear stress were linearly related in a bare-bed channel. In the vegetated channel flows, however, vegetation stems predominate the production of the turbulence (Tanino & Nepf, 2008); thus the shear stress is no longer alternative to the near-bed turbulence, that is, the turbulent kinetic energy. Recently, many studies have attempted to prove the effect of turbulence on the incipient sediment motion (Diplas et al., 2008; Tang et al., 2019; Yang et al., 2016). For example, according to the study of Yang et al. (2016), the depth-averaging critical velocity in the vegetated channels was estimated as follows:

$$U_c = \frac{U_{c0}}{\sqrt{1 + \frac{\delta^2}{C_b} \left(\frac{2C_D\phi}{\pi(1-\phi)} \right)^{2/3}}}, \quad (15)$$

where U_{c0} [LT^{-1}] and U_c [LT^{-1}] denote the depth-averaging critical velocity in the bare bed flow and the vegetated flow, respectively; coefficient $C_b = C_f/2$ [-] (C_f is the bed friction coefficient); and δ [-] is a scale factor.

The sediment resuspension probability is derived from the critical velocity of the incipient sediment motion and the probability density function of the instantaneous flow velocity. As expressed in Equation 15, the depth-averaging velocity is most commonly used as the criterion for the sediment incipient motion.

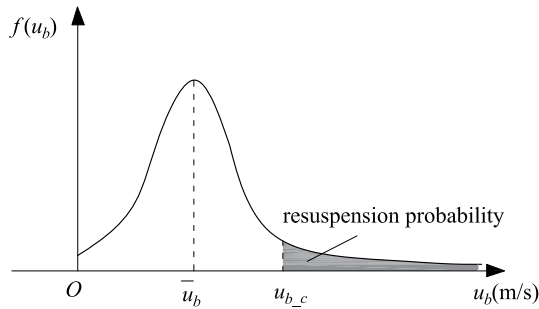


Figure 4. Probability density function of u_b and the diagram of the resuspension probability.

Dou (1960) derived the following formula of the sediment incipient motion based on the balance of forces acting on the sediment particle:

$$U_c = 0.408 \left(\ln \left(\frac{H}{k_s} \right) \right) \left((s-1)gd_{50} + 0.19 \frac{\varepsilon_k + gH\delta_p}{d_{50}} \right)^{1/2}, \quad (16)$$

where g [LT^{-2}] is the acceleration due to gravity; d_{50} [L] is the median size of the sediment particles; $k_c = 1.437$ is a constant parameter; s [-] is the ratio of the bulk sediment density over water density; $\delta_p = 0.213 \times 10^{-6}$ [L] is the thickness of pellicular water; k_s [L] is the roughness height of bed ($k_s = 0.0005$ m if $d_{50} < 0.5$ mm); and ε_k [L^3T^{-2}] (usually taken as $2.56 \times 10^{-6} m^3s^{-2}$) is a comprehensive parameter of cohesive force.

Previous studies showed that the depth-averaged velocity was a valid criterion for the majority of sediments onset motion. However, the present model pays more attention to the motion of each single particles, especially

in the region near the bed. Therefore, it is more accurate to take the near-bed velocity, instead of the depth-averaged velocity, as the criterion for the sediment onset motion. The different turbulent intensity leads to a variation of the probability density function of the flow velocity at the vegetation and overflow regions (Nezu & Nakagawa, 1993). As such, the velocity near the bottom of the channel, u_b , is used as the criterion to determine whether the sediment resuspension occurs or not (Marion & Tregnaghi, 2013). The sediment at the position of two times sediment particle size above the channel bed is regarded as the suspended sediment. Therefore, the flow velocity at $z = 2d_{50}$ is assumed as the near-bed flow velocity u_b . The critical depth-averaging flow velocity, Equation 16, is then transformed to the critical near-bed velocity, $u_{b,c}$, according to the rate of the depth-averaging velocity and the near-bed velocity on the exponential velocity profile:

$$u_{b,c} = 0.476(2d_{50})^{1/6} H^{-7/6} \left(\ln \left(\frac{H}{k_s} \right) \right) \left((s-1)gd_{50} + 0.19 \frac{\varepsilon_k + gH\delta_p}{d_{50}} \right)^{1/2}. \quad (17)$$

The critical near-bed velocity, $u_{b,c}$, calculated by Equation 17 will be used to determine the inception of the sediment resuspension. To clarify the relationship between the turbulent kinetic energy induced by the vegetation and the sediment resuspension, we analyze the simulated results and the variation of the turbulent kinetic energy that actually affects the variation of the flow velocity.

The incipient motion criterion, that is, the critical velocity, is transformed into the resuspension probability of the sediment particles according to the instantaneous velocity fluctuations, which approximates to the Gaussian profile. The sweeps and ejections, which lead to highly non-Gaussian profile, usually occur in the mixing layer and reach the maximum at the top of vegetation (Huai, Zhang, et al., 2019; Okamoto et al., 2012). In the present study, we adopt the flow velocity at $z = 2d_{50}$, where ejections and sweeps are weak, as the near-bed velocity, u_b . In this way, u_b is approximate to the normal distribution (Choi & Kwak, 2001), and the probability density function of u_b can be derived as follows:

$$f(u_b) = \frac{1}{\sqrt{2\pi}\sigma} e^{-\frac{1}{2} \frac{(u_b - \bar{u}_b)^2}{\sigma^2}}, \quad (18)$$

where \bar{u}_b [LT^{-1}] is the time-averaging near-bed flow velocity and $\sigma = \sqrt{(u_b - \bar{u}_b)^2}$ is the standard deviation in which $\sigma = 1$ is usually used. When the instantaneous velocity is larger than the critical velocity of the incipient motion, the resuspension of the sediment particles takes place, as shown in Figure 4. The resuspension probability P_s , therefore, can be simulated as follows:

$$P_s = 1 - P(u_b < u_{b,c}) = 1 - \int_{-\infty}^{u_{b,c}} \frac{1}{\sqrt{2\pi}\sigma} e^{-\frac{(u_b - \bar{u}_b)^2}{2\sigma^2}} du_b. \quad (19)$$

In the present model, sediment particles reaching the channel bed firstly deposit according to the deposition probability model, and then some are re-suspended according to the resuspension probability model. From the model and resuspension concept, the deposition motion is the foundation of resuspension motion.

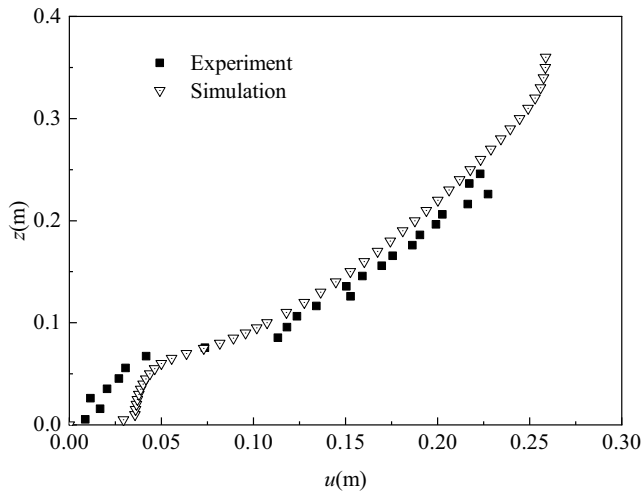


Figure 5. Comparison of the simulated and measured longitudinal velocity at position $x = 5$ m.

We assume that the resuspension probability is a constant calculated by Equation 19 in the whole domain and therefore, we emphasize the effect of deposition probability to study the main factors that impact the net deposition, that is, deposition probability.

3. Results

The numerical modeling procedure mainly includes three steps: (a) the flow field is modeled with the realizable $k-\epsilon$ model and porous model; (b) the RDM is performed using governing equations of sediment particles motion, that is, Equations 1 and 2, associating with the calculated flow field data in the first step and the simplified turbulent diffusion coefficient; and (c) the value of unknown deposition probability P_{d1} is fitted through the comparison of the simulated deposition and experimentally measured deposition. The proposed model is then applied to simulate the deposition of the sediment particles in the vegetated channel flows and is validated by comparing the simulated results with the measurements in several available laboratory experiments, which are briefly described below.

3.1. Validations

3.1.1. Flow Field

The experiments conducted by Zhang et al. (2020) are used to verify the flow field model. Zhang et al. (2020) conducted experiments to study the sediment deposition profiles in the submerged long meadows for different flow and vegetation density conditions. The numerical domain is chosen as a 0.36 m high and 10 m long 2-D region. The vegetation zone is 0.07 m high and 8.4 m long. In the model, the finest mesh size is 5×5 mm² in the vegetation zone. Taking Case 3 as an example, mainly experimental parameters are: $H = 0.36$ m; $h = 0.07$ m; $U = 0.16$ m/s; $U_1 = 0.04$ m/s; $\phi = 0.048$, $C_D = 1.3$, $x_D = 0.80$ m, and $x_p = 4.65$ m; where U [LT⁻¹] is the depth-averaging flow velocity and U_1 represents the mean longitudinal velocity within vegetation region.

Figure 5 shows the good agreement between the simulated and measured longitudinal velocity u at position $x = 5$ m. In the vegetation region, the simulated longitudinal velocity is slightly larger than the experimental data. Although the porous model could simulate the effect of vegetation by adding extra drag force, the absence of real structure of vegetation weakens the impact of vegetation, which is likely to account for the overestimation of the modeled velocity in the vegetation zone. This means that the decrease of velocity with the impact of the vegetated obstacle in the present model is weaker than experiments. Nevertheless, the proposed model could accurately reproduce the main flow characteristics in channels with submerged meadows.

Figure 6 demonstrates the modeled u and w , where the dash lines express the vegetation zone. It is seen that u decreases within the region of vegetation, while the velocity of overflow is accelerated (Figure 6a). The vertical diversion takes place near the head of vegetation patch, as shown in Figure 6b. Good agreement between the simulation and measurement indicates that the porous and realizable $k-\epsilon$ models perform well on the simulation of the flow field in the channel with submerged vegetation.

3.1.2. Deposition Probability Model

Sediment transport (deposition and resuspension) is calculated using the RDM associating with the calculated flow field and simplified turbulent diffusion coefficient. In the simulation, 500,000 particles are modeled with the time step of 0.05 s. In the RDM, the condition at the outlet is assigned as the inlet condition at the next time-step in the computational domain to simulate the sediment transport in the cyclic flume. This means that the sediment particles that pass through the outlet will return back into the inlet and transport in the flume again. The present study models the sediment net deposition in the channel with both the submerged and the emergent vegetation, respectively.

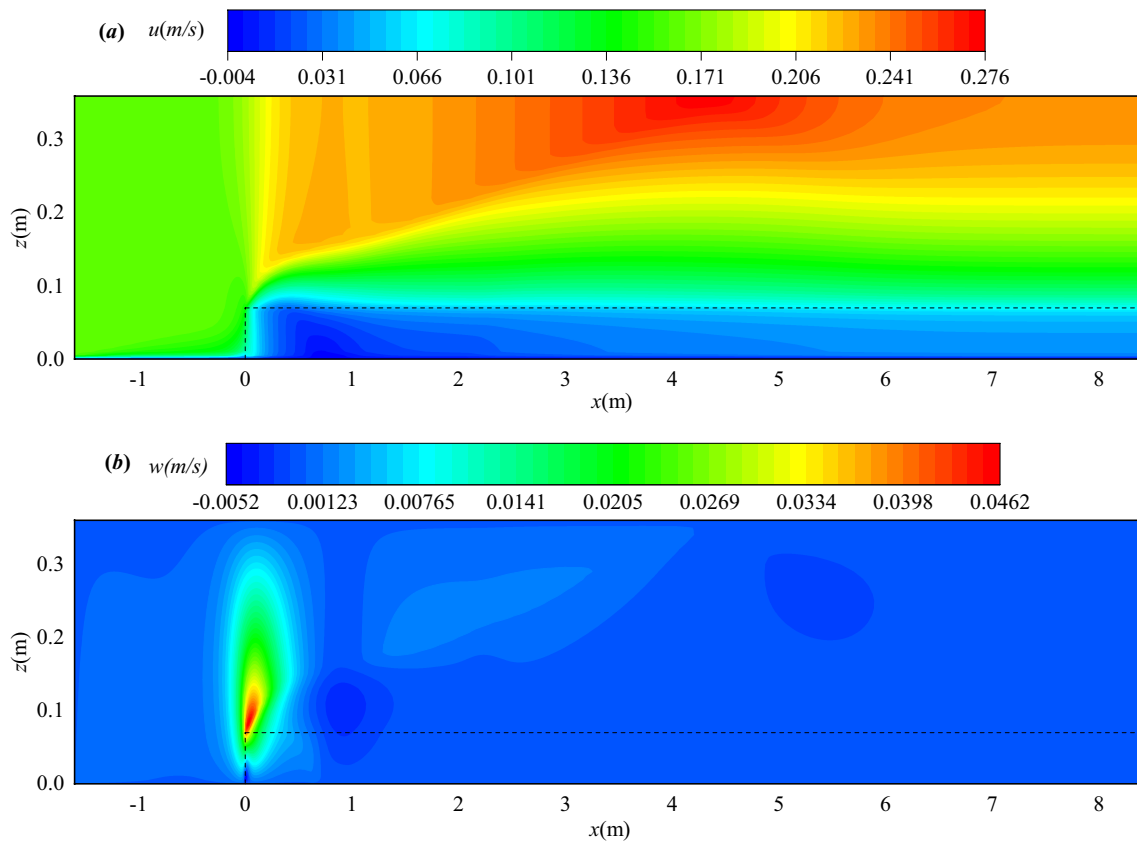


Figure 6. Contour plot of the simulated longitudinal and vertical velocity.

To determine which deposition probability (Equations 12–14) provides better prediction, the simulated sediment net deposition is compared with the experimental measurements. Figure 7 shows the results of the simulated net deposition with three probability profiles (Equations 12–14), taking Case 4 (see Table 2 in Section 3.2) as an example. The mean-root error, calculated as

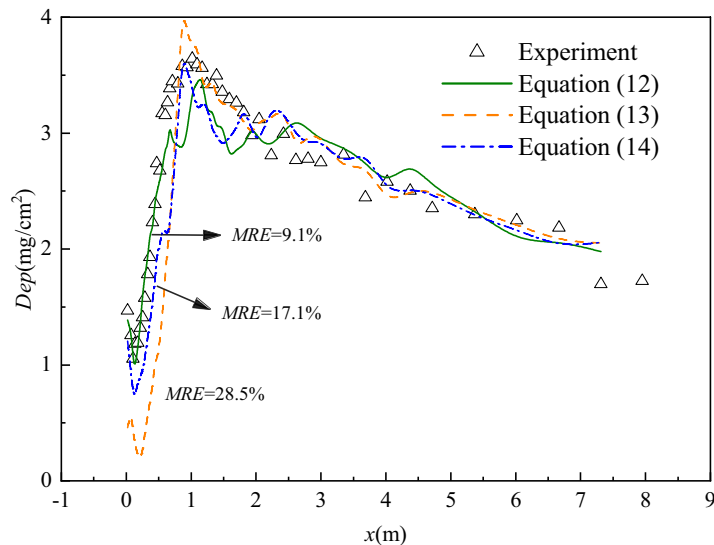


Figure 7. Comparison of the experimentally measured net deposition in Zhang et al. (2020) and simulated deposition with three assumed deposition probability profiles.

Table 1
Experimental Parameters in the Study of Zong and Nepf (2010)

Conditions	H (m)	U (m/s)	ϕ (-)	x_D (m)	x_p (m)	M_{tot} (g)	P_{d1} (%)
Z-Dense	0.14	0.005	0.1	2	7.5	86	1
Z-Sparse	0.14	0.014	0.02	3	7.5	95	1

$MRE = \frac{1}{N} \sum \left(\frac{|Dep_e - Dep_m|}{Dep_e} \right) \times 100\%$ (where Dep_e and Dep_m [ML^{-2}] are experimental and modeled net deposition respectively and N [-] is the observation number of deposition) is also plotted in Figure 7. It is shown that the MRE with Equation 12 is the smallest within the three profiles, indicating that the sediment net deposition simulated with Equation 12 is more accurate. Therefore, the deposition probability is expressed as

$$P_d = \begin{cases} -\frac{P_{d1}}{x_D^2} x^2 + \frac{2P_{d1}}{x_D} x & x \leq x_D (20 - a) \\ P_{d1} & x > x_D (20 - b) \end{cases}$$

3.2. Sediment Deposition

Zong and Nepf (2010) conducted experiments to study the effect of the dense and sparse emergent vegetation on the sediment deposition with vegetation covering half-wide channel. Their experimental parameters are listed in Table 1, where M_{tot} [M] is the total deposition in the vegetation region. However, the present study does not focus on the lateral profile of the sediment deposition. Instead, we mainly study the deposition patterns along the streamwise direction. The deposition in the center line of vegetation region is approximately thought as the deposition in channel with vegetation, as the main effect region of lateral diversion, that is, outer region, excludes the center line of vegetation, see Figure 5 in Zong and Nepf (2010). Figure 8 shows the comparison of the simulated and experimentally measured sediment deposition, where Dep [ML^{-2}] represents the deposition per unit area. It is seen from Figure 8 that the sediment deposition profile predicted by the proposed model generally agrees with the experimental measurements, which validates the reliability and accuracy of the proposed model. This also means that the proposed deposition and resuspension probability in this study can appropriately reflect the effect of the flow field on the sediment net deposition in the channel with the aquatic vegetation.

Figure 9 shows the comparison of the simulated sediment deposition profile with the laboratory experiments conducted by Zhang et al. (2020) (see Table 2 experimental parameters in each case) in the meadow along the longitudinal direction. Zhang et al. (2020) focused on investigating the effect of the flow velocity and the vegetation density on the sediment net deposition in the vegetation region. For the sake of convenience, the related conditions, such as the vegetation density and the depth-averaging velocity, are also shown in Figure 9.

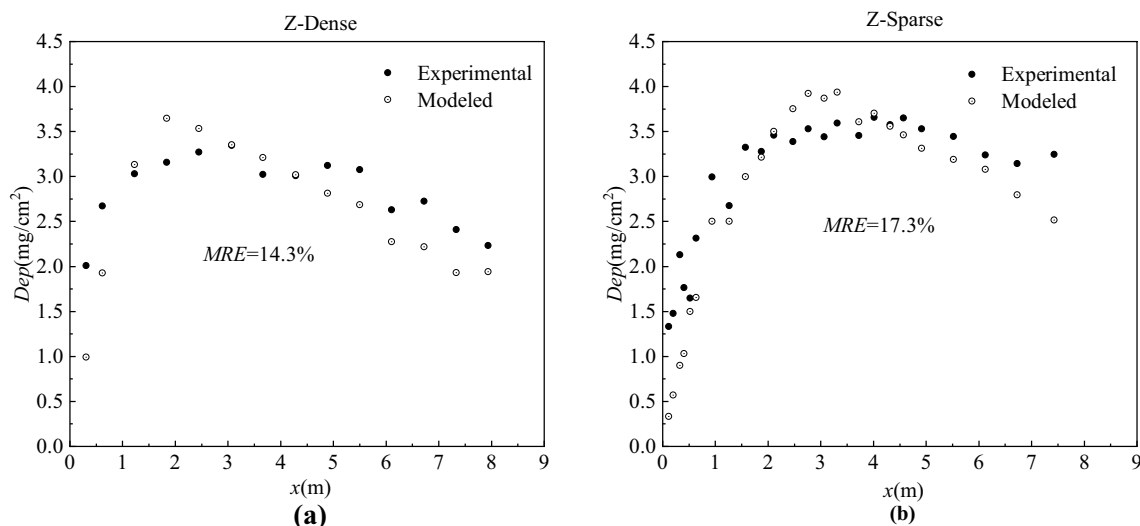


Figure 8. Comparison between the experimentally measured and modeled sediment deposition profiles within the vegetation patch region in the open channel flows. (a) Dense vegetation patch and (b) sparse vegetation patch.

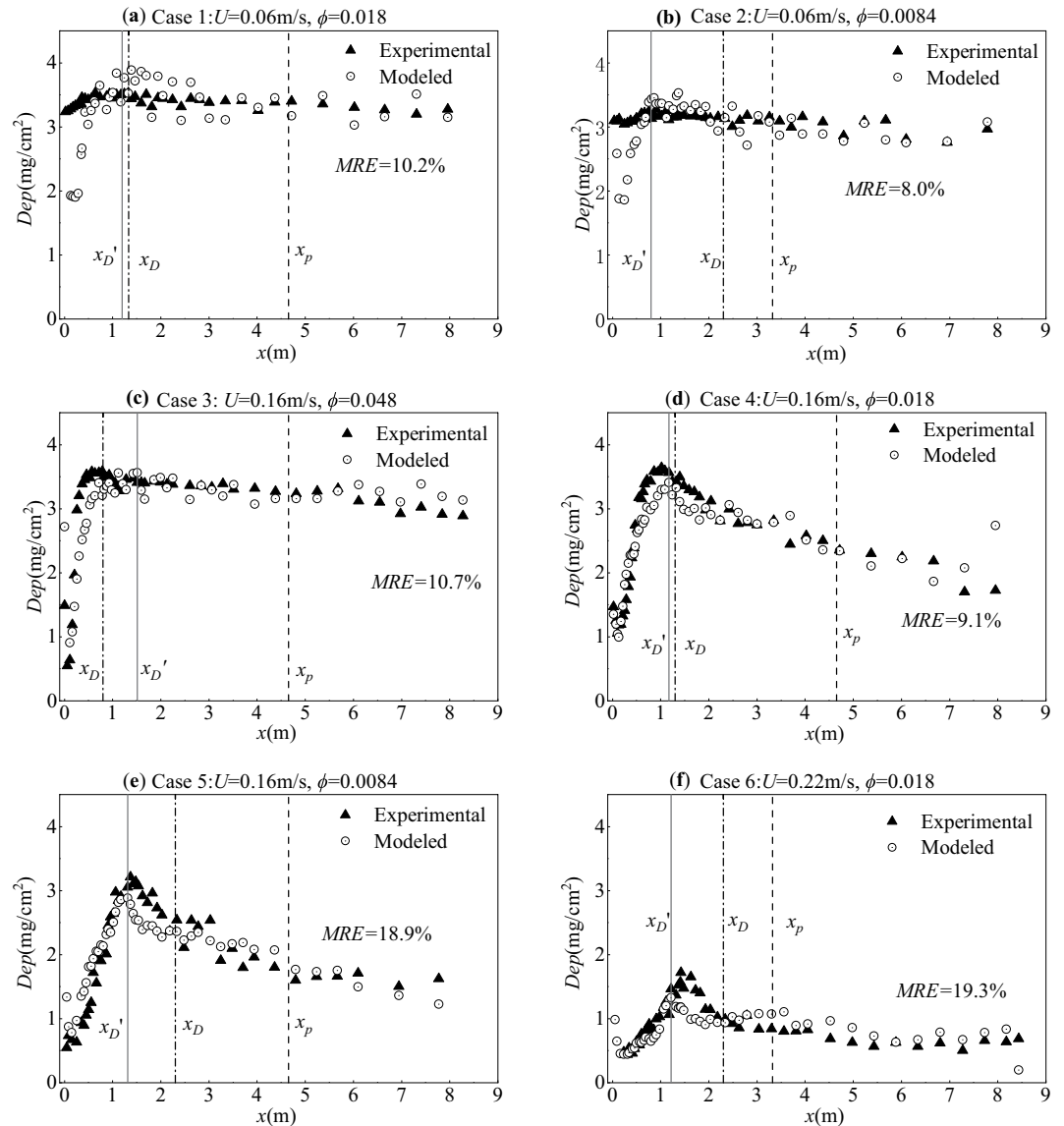


Figure 9. Predicted and experimentally measured sediment deposition profiles. The vertical solid lines show the position of the maximum sediment deposition ($x_{D'}$) in the model; while the dot dash lines and dash lines are the end of the adjustment (x_D) and transition regions (x_p), respectively, and the two lines divide the vegetation patch into three parts.

The results in Figure 9 show that the sediment net deposition is small in the leading edge of the meadow due to the effect of updraft. This net sediment deposition then increases sharply with the increase of the longitudinal distance within a small leading edge region. For Cases 1 and 2, the sediment resuspension probability is slightly different from other conditions. Table 2 shows that the velocity for these two cases is much smaller than those of others; therefore, the turbulence intensity is also small. As a result, the effect of the vegetation on the resuspension is trivial. This leads to a zero resuspension probability, which is also confirmed by Zhang et al. (2020). Figure 9 also shows that the simulated net deposition is smaller than experimental measurements in the upstream of vegetation. According to the analysis of Zhang et al. (2020), for Cases 1 and 2, with the lowest velocity, net deposition profiles in vegetation region are the same as the deposition outside vegetation, that is, spatially uniform pattern. This implies that the effect of vegetation updraft on the deposition patterns is trivial in these conditions. However, the deposition probability model proposed in this study considers the impact of updraft through the gradually increased deposition

Table 2
Experimental Parameters of Zhang et al. (2020)

Conditions	H (m)	h (m)	U (m/s)	U_1 (m/s)	ϕ (-)	C_D (-)	x_D (m)	x_p (m)	M_{tot} (g)	P_{dl} (%)
Case 1	0.36	0.07	0.06	0.02	0.018	1.4	1.33	4.65	106	2
Case 2	0.36	0.07	0.06	0.03	0.0084	1.3	2.30	3.32	96	2
Case 3	0.36	0.07	0.16	0.04	0.048	1.3	0.80	4.65	101	5
Case 4	0.36	0.07	0.16	0.07	0.018	1.2	1.30	4.65	79	40
Case 5	0.36	0.07	0.16	0.09	0.0084	1.1	2.30	4.65	61	50
Case 6	0.26	0.07	0.22	0.13	0.0084	1.1	2.30	3.32	25	20

probability for all conditions, which may account for the deposition difference between model and experiment in the leading of vegetation.

Overall, the simulated net deposition is consistent with the measurements, especially in the region $x > x_D$. The deviation is more likely to be found in the updraft region, where the vertical flow velocity is stronger than that in the developed region. Although the complex flow structure in the adjustment region complicates the modeling, the net deposition is still well simulated by the proposed model. Furthermore, the simulated results illustrate that both the magnitude and position of the predicted maximum sediment deposition are reasonably consistent with the experimental measurements, although some deviation exists in the simulated and experimental positions where the deposition reaches the peak (e.g., Case 3 shown in Figure 9c). Except for Case 3, the position x_p' , where the simulated sediment deposition reaches the peak value, is always ahead of the adjustment region length x_D derived by Chen et al. (2013). These results indicate that the vertical updraft seems to disappear ahead of the calculated x_D , which was also confirmed by the results shown in Figure 3b in the study of Follett and Nepf (2018). Therefore, it can be concluded that the net deposition reaches the maximum value ahead of x_D .

The total deposition in Cases 1, 2, and 3 is larger than that in Cases 4, 5, and 6, while the deposition probability of Cases 1, 2, and 3 is considerably smaller than that in Cases 4, 5, and 6. This phenomenon may be ascribed to two facts. First, for Cases 1 and 2, although the sediment deposition probability is small due to small flow velocity and weak turbulence intensity, the resuspension rarely exists under the effect of the weak turbulence, leading to the large total deposition. In these conditions, the effect of the vegetation and the shear stress on the sediment deposition is comparable. Second, on the one hand, with the bulk velocity of Case 3 increasing to the same magnitude of Cases 4, 5, and 6, the turbulent intensity is no longer small than that in the other cases. In this situation, the aquatic vegetation plays an important role on the deposition, which is dramatically different from the low current condition. This means that the deposition probability is small because of the strong turbulence. On the other hand, dense vegetation, which means more obstructions, generates small sand-carrying capacity of flow and large net deposition, as verified by Cases 3, 4, and 5 (deposition increases with the increase of the vegetation density). These discussions have well explained that net deposition of Cases 1, 2, and 3 is large while their deposition probability is small.

3.3. Relevance of the Turbulent Kinetic Energy to Sediment Motions

The turbulent kinetic energy is used as a characteristic parameter of the turbulence to explore the relationship between the net sediment deposition/resuspension and the turbulent intensity. As discussed above, the sediment incipient motion is closely related to the turbulent kinetic energy. This is because the turbulence dominates the sediment transport in the vegetation region in the vegetated sediment-laden flow; while in the bare-bed channel flow, it is the shear stress that determines the sediment transport. According to the study of Tanino and Nepf (2008), the vegetation-induced turbulent kinetic energy, k [L^2T^{-2}], can be expressed as follows:

$$k = \delta^2 \left(\frac{2C_D\phi}{\pi(1-\phi)} \right)^{2/3} U^2. \quad (21)$$

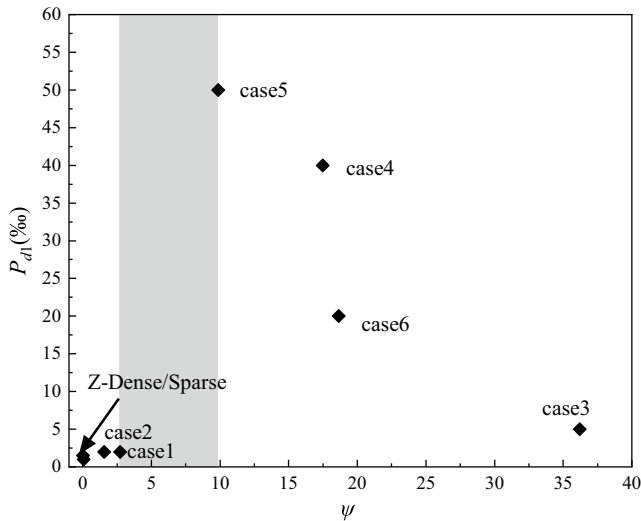


Figure 10. Variation of the sediment deposition probability (represented by the deposition probability outside the adjustment region P_{d1}) with the dimensionless turbulent kinetic energy ψ . The gray block indicates the scope of the critical turbulent kinetic energy.

The scale factor $\delta = 1.1$ is used in this study when the ratio of the vegetation stem diameter and the mean interval between stems is smaller than 0.56 (Tanino & Nepf, 2008). The sediment motion in the flow is closely related to the sediment intrinsic characteristic, such as sediment size or relative density, and flow characteristics, such as flow velocity or turbulent kinetic energy. To analyze the relationship between turbulent kinetic energy and sediment motion, the turbulent kinetic energy can be normalized by the characteristic parameter of the sediment particles, that is, $(s-1)gd_{50}$, which is similar to the method of the Shields number. The dimensionless turbulent kinetic energy ψ can then be written as follows:

$$\psi = \frac{\delta^2}{(s-1)gd_{50}} \left(\frac{2C_D\phi}{\pi(1-\phi)} \right)^{2/3} U^2. \quad (22)$$

3.3.1. Relevance to Deposition

Figure 10 shows the variation of the deposition probability P_{d1} with the dimensionless turbulent kinetic energy ψ , demonstrating the effect of the turbulence induced by the vegetation on the sediment deposition. It is seen from Figure 10 that the deposition probability decreases with the increase of the turbulent kinetic energy when ψ ranges from 10 to 37 according to the conditions of Cases 3, 4, 5, and 6. This situation can be explained by the effect of the vegetation-induced turbulent kinetic energy on the sediment movement. The sediment deposition is inhibited

by the intense turbulence, as found in the study of Kim et al. (2018). This phenomenon can be explained by the underlying mechanisms of sediment deposition and resuspension. The close relationship between the sediment movement and the flow field features indicates that the strong turbulent vortex enhances the sediment resuspension and weakens the sediment deposition. Furthermore, the sediment particles usually move upward due to the vortices induced by the vegetation (Tinoco & Coco, 2016). Therefore, both the sediment concentration near the channel bed and the virtual deposition layer decrease. Engelund and Fredsoe (1976) showed that the incipient sediment motion did not complete at a moment; by contrast, the upper sediment was easily suspended by the flow. From this aspect, the reduction in the upper layer, $\Delta C(t, x, dz/2)$, is larger than that in the virtual deposition layer, $\Delta C(t, x, -dz/2)$, when turbulent intensity is enhanced, that is, ψ increases. As a consequence, the sediment deposition probability is smaller compared with the deposition probability in the condition of the weak turbulent kinetic energy according to Equation 9.

For conditions “Cases 1 and 2, Z-dense and Z-sparse,” represented by “Small case” hereafter, the flow velocity and the stem Reynolds number are much smaller than that in Cases 3, 4, 5, and 6 (see Tables 1 and 2). The deposition probability $P_{d1} = 1‰$ or $2‰$ for the “Small cases” is quite similar to that in the channel without vegetation, and the corresponding turbulent kinetic energy is in the range $0 < \psi < 2.5$. The weak turbulence intensity induced by small velocity and the stem Reynolds number has a weak impact on the sediment deposition and the resuspension comparing with the situation in the bare-bed channel flow. The deposition probability is the same as that in the bare-bed channel, and the net sediment deposition profile is nearly a flat level in the vegetation patch region. In the “Small cases,” the increased turbulent kinetic energy cannot enhance the sediment deposition probability, indicating that there exists a critical value of ψ before the impact of the canopy-induced turbulent kinetic energy, which dominates the sediment motion. The result shows that the critical value of ψ , represented as ψ_c , is from 2.5 to 10.

The above analysis shows that the flow velocity and the vegetation density are the main factors affecting the turbulent kinetic energy (see also Equation 22). However, the present study shows that these two factors probably affect the turbulent kinetic energy in different ways. The depth-averaging flow velocity represents the state of the whole current movement and plays a more important role on the turbulent kinetic energy than that played by the vegetation density, as indicated by the different indices of U and ϕ in Equation 22. The results of the present study suggest that if the velocity is small (e.g., similar to the “Small cases”), the effect of the vegetation on the deposition is then minimal no matter it is dense or sparse vegetation. When the flow velocity is sufficiently large to generate the strong turbulence, the vegetation effect starts to become

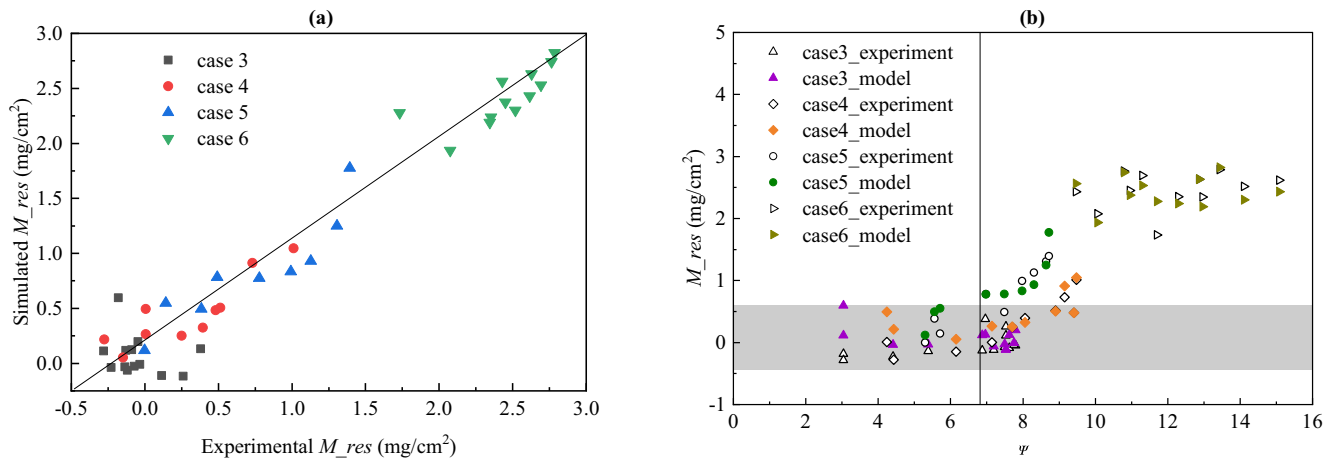


Figure 11. (a) Comparison of experimentally measured and simulated resuspension; (b) relationship between the resuspension and the dimensionless turbulent kinetic energy. The gray square expresses the extent where the impact of the turbulent kinetic energy is insignificant.

significant. The deposition probability decreases continuously with the increase of the vegetation density as illustrated by Cases 3, 4, and 5, as shown in Figure 10.

3.3.2. Relevance to Resuspension

The particles resuspension motion could be promoted by the turbulence. Zhang et al. (2020) took the deposition in Cases 1 and 2 (3.24 ± 0.16 mg/cm²) as the inferred deposition without resuspension, and calculated the sediment resuspension according to the deviation between measured net deposition and this inferred deposition. Adapting the same method as Zhang et al. (2020), Figure 11 shows the comparison of the simulated and measured resuspension, M_{res} [ML⁻²] (Figure 11a), and the relationship between the resuspension and dimensionless turbulent kinetic energy, ψ (Figure 11b). Good agreement between the simulated and experimentally measured resuspension further verifies the present model. From Figure 11b, the resuspension is small for $\psi < 6.8$ and then increases with the increase of the turbulent kinetic energy. This implies that there exists a critical turbulent kinetic energy, that is, $\psi^* = 6.8$ in this study, which is also within the range of the threshold inferred from analysis about deposition and ψ (see Figure 10). Considering the relationship between both the deposition and resuspension with the turbulent kinetic energy, the critical ψ can be further estimated as $6.8 < \psi^* < 10$. This means that when the turbulent kinetic energy is above the threshold, the turbulence induced by vegetation dominates the sediment particles motions, namely the deposition and resuspension.

4. Discussion

A probability model of the sediment deposition and the resuspension is proposed in this study. The net sediment deposition in the flow with the vegetation patch is simulated by integrating the probability model with the RDM. The results show that the turbulent kinetic energy has a more remarkable effect on the sediment deposition and the resuspension than the bed shear stress in the vegetated sediment-laden flow. The results also indicate that the effect of the aquatic vegetation on the sediment deposition seems to be significant when the turbulent kinetic energy is larger than the threshold. The present study fills the knowledge gap by integrating the sediment deposition probability and the turbulent kinetic energy. Furthermore, this study also extends the application of the RDM to the study of the sediment deposition in the channel with vegetation, though there are several inevitable limitations for the RDM.

4.1. Probability-Based Boundary Model

The deposition boundary used in this study refers to the sorption boundary of the pollutant (Wang & Huai, 2019). The simulated net deposition agrees well with the experimental measurements because the sediment particles in the present study are small, that is, $d_{50} = 7$ μ m in the study of Zhang et al. (2020) and

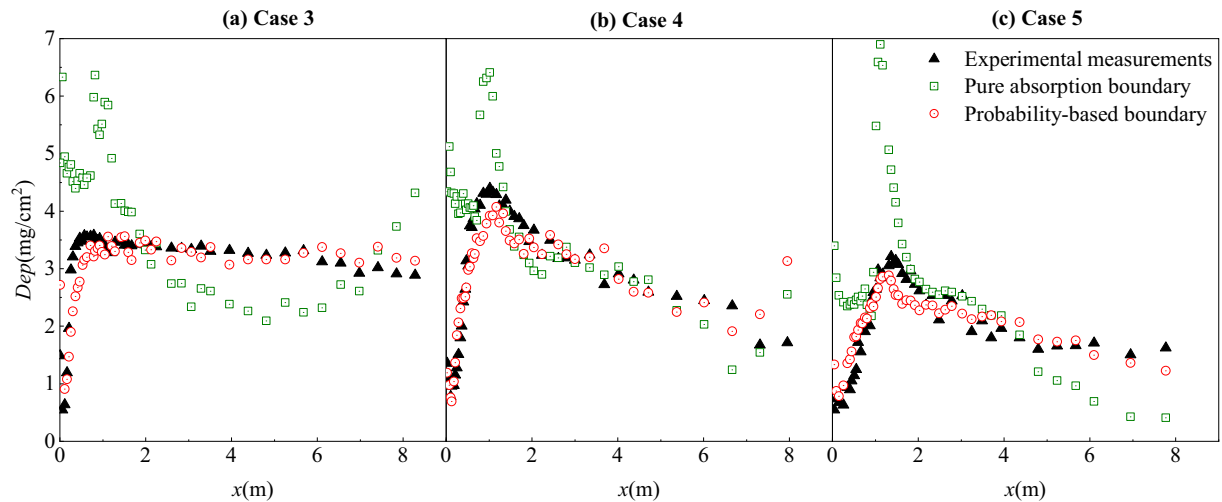


Figure 12. Comparison of the experimentally measured deposition (black solid triangles) and the simulated deposition patterns with the pure sorption boundary (green open squares) and the probability-based boundary (red open circles).

$d_{50} = 12 \mu\text{m}$ in the experiments of Zong and Nepf (2010). The approach as to whether settling velocity is considered or not is the main difference between the sediment and the pollutant whose settling velocity is usually ignored. Therefore, the transport of fine sediments may be similar to that of the pollutant because the settling velocity is small. Figures 8 and 9 show that the deviation between the simulated and measured deposition in the experiment of Zong and Nepf (2010) is larger than that in the experiments of Zhang et al. (2020), which could be due to the difference in the sediment diameter in these two experiments. Furthermore, the whole variation tendency of the observed deposition in the experiments of Zong and Nepf (2010) along the streamwise direction in the downstream of the adjustment region is much flatter than the simulated deposition. This result demonstrates that the particles diameter has an effect on the accuracy of this model. Overall, the model proposed in this study is applicable to the fine sediment as the approach of the deposition boundary is a progress in the theory of sorption boundary for pollutant.

To simulate the sediment motion characteristics, that is, deposition and resuspension, we adapt the pure sorption boundary to probability-based boundary. Taking Cases 3, 4, and 5 as examples, Figure 12 shows the comparison of the sediment deposition patterns with the pure sorption boundary and the probability-based boundary, respectively. The pure sorption boundary ignores the fact that the sediment particles, which temporarily reach the channel bed, could not stay there completely and the majority of the sediment particles will be transported away from the channel bed by turbulence. Therefore, the pure sorption boundary poorly models the sediment deposition in the channel with canopy. However, the probability-based boundary model takes this instability of particles motion into account with the probability model adapting to the flow field structure. In addition, there is large modeled deposition deviation between the probability-based and the sorption boundary in the leading of vegetation, indicating that the impact of updraft in the adjustment region plays an important role in the sediment motion. The comparison reveals the superiority of the present model in simulating the sediment deposition in channels with vegetation.

The probability model proposed in this study can reveal the interaction between the vegetation and the sediment deposition and resuspension. The resuspension probability is derived from the probability density function of the near-bed averaging flow velocity, while the deposition probability must be calibrated by experimental data. To better describe the deposition probability, sufficient experimental data are required. Although the experimental data are limited, this study illustrates several findings through analyzing the dimensionless turbulent kinetic energy and investigating the relationship between the sediment deposition probability and the turbulent kinetic energy. The analysis shows that within the scope of ψ investigated in this study, the deposition probability decreases with the increase of the turbulent kinetic energy when the turbulence kinetic energy is larger than its threshold. The effect of the vegetation on the sediment deposition prevails when the turbulent kinetic energy is larger than the critical value. However, the problem has

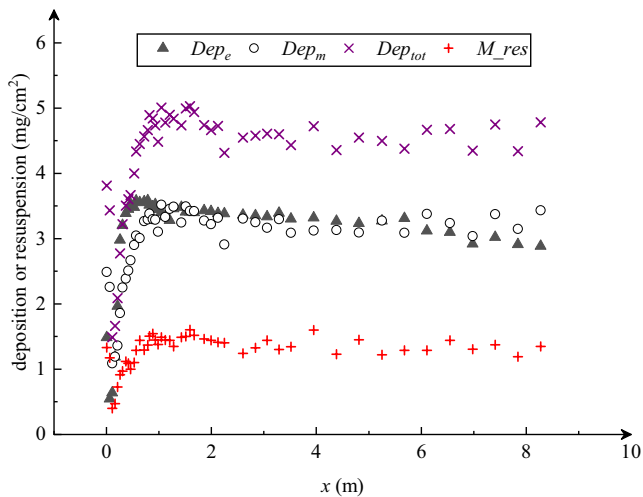


Figure 13. Deposition measured in the experimental Case 3, Dep_e (gray triangles); simulated deposition Dep_m (circles) with resuspension; total deposition Dep_{tot} (purple forks) without resuspension; and the simulated resuspension M_{res} (red crosses).

not been quantitatively analyzed; and the formula used to determine the deposition probability, which is acknowledged difficult to overcome, is not derived due to the limited experimental data. Further experiments are also required to explore the relationship between sediment motions and the turbulent kinetic energy.

4.2. Particles Motions

The calculated resuspension conducted in Zhang et al. (2020) is a relative value, which means that all calculated resuspension is relative to the averaged deposition in Cases 1 and 2. They explained that the resuspension motion accounted for the lower deposition in other cases. The method could, to some extent, show the effect of flow field characteristics on the deposition and resuspension within the experimental period (e.g., 4 h in the experiment) through analyzing the relative value in different conditions. However, it is difficult for the method to clarify the process of sediment particles deposition and resuspension motions. In the present study, the numerical model, that is, the RDM, tracks particles motion; the deposition and resuspension could be clarified through accounting the number of deposition and resuspension particles, respectively.

Taking Case 3 as an example, Figure 13 shows the total deposition without resuspension, measured and modeled deposition with resuspension, and the simulated resuspension. The validity of the model has been discussed above, therefore, we expect to infer sediment particles motion from the model. According to the present model, the deposition probability in the leading of head is small with the effect of updraft, while the resuspension probability, calculated from the near-bed velocity, is a constant in the whole domain. Figure 13 shows that the pattern of resuspension along the longitudinal direction is the same as the deposition without resuspension, although the pattern of deposition and resuspension probability is different from each other in the adjustment region. It is also found that the magnitude of deposition is larger than resuspension. The result indicates the effect of the deposition motion on the pattern of final deposition is relatively more important than resuspension motion. The experiments of the sediment deposition discussed in this study were conducted by feeding sediment in the upstream of the flume. This means that particles deposition in the bed is the precondition of resuspension. Therefore, the finding is consistent with the concept of resuspension. For another experiment method, i.e., paving sediment layer in the channel bed (Tinoco & Coco, 2016), it is obvious that resuspension dominates the sediment particles motion, and the deposition was ignored in the study. The different experimental methods may interpret two completely different findings between the present study and Tinoco and Coco (2016). From the results of the present model, it is important for the resuspension analysis to clarify its definition.

4.3. Random Displacement Model

The RDM has been successfully applied to simulate the vertical profile of the suspended sediment concentration in the fully developed state (Huai, Yang, et al., 2019). The boundary condition at the channel bottom proposed in this study associates the deposition and resuspension probability model and further expands the application of the model in the study of sediment deposition within the aquatic vegetation region, which may considerably promote the development of the sediment deposition studies.

Though the RDM has been successfully applied to simulate the sediment transport in the vegetated channel in this study, there are still some limitations in RDM, which have already been discussed by Wilson (2000). In this study, we briefly discuss the limitations of RDM, mainly based on the present study objectives. First, it is difficult for RDM to simulate the dispersion properties in the near field of the channel bed. In the channel with vegetation, the vortex induced by vegetation stems and the channel bed cannot be reproduced by RDM. Comparing with the previous study, Duman et al. (2016) tracked heavy particles motion in the canopy sublayer with the generalized Lagrangian method to study the long-distance dispersal of heavy particles.

This model could accommodate all the turbulent velocity components, which benefits to link the turbulent kinetic energy to resuspension and deposition. Besides, the flow field used in the RDM is time-averaged, which cannot simulate the velocity fluctuations. In contrast, the velocity evolves in time according to a generalized Lagrangian equation. However, in this study, the flow field is much more complex, especially in the leading of vegetation meadow. For such complex flow situation, application of the generalized Lagrangian approach is difficult as many parameters, for example, velocity fluctuations, need to be calibrated. In the present study, we focus on examining the effect of the probability-based boundary model on the deposition and attempt to find the relationship between the deposition and the turbulent kinetic energy. We have to control the number of variables to ensure the reliable results. Therefore, although the model fails to reproduce the dispersion properties in the near field of the channel bed, it has little effect on achieving the objectives of this study. Furthermore, the application of the bottom boundary conditions in this study has, to some extent, compensated the limitation of the RDM in the near field of the channel bed, which is evidenced by the good agreement obtained between the simulated and measured net deposition. As such, considering the simplicity and physical plausibility, the RDM is a good method for investigating the sediment transport in vegetated channels.

5. Conclusions

This study simulates the profile of the net sediment deposition in the vegetation patch and focuses on investigating the effect of the turbulent kinetic energy on the deposition probability through an innovative RDM. The deposition probability increases from zero at the leading edge of the vegetation patch ($x < x_D$) and maintains a constant value at the region $x > x_D$. The resuspension probability is derived from the probability density function of the flow velocity near the channel bed by assuming that the sediment resuspension occurs when the instantaneous velocity is larger than the critical velocity of the incipient sediment motion. The following conclusions can be drawn from this study:

- (1) The sediment deposition probability is closely related to the turbulent kinetic energy ψ . The effect of the turbulent kinetic energy induced by the aquatic vegetation on the sediment deposition is similar to the effect of the shear stress in the bare-bed channel when ψ is small. By contrast, the turbulent kinetic energy dominates the sediment deposition when the value of ψ is larger than the critical value ψ_* , and the deposition probability decreases with the increase of ψ for $\psi > \psi_*$.
- (2) The threshold of the turbulent kinetic energy ψ_* is an important parameter in the deposition studies because the effect of the vegetation on the sediment deposition and resuspension begins to prevail when $\psi > \psi_*$. In the present study, the threshold cannot be derived directly due to the limited experimental data; however, the range of 6.8–10 is recommended as the critical value based on the analysis of the simulation. Further experiments are needed to determine the specific threshold of the turbulent kinetic energy.
- (3) The innovative RDM proposed in this study extends the application of the model on the sediment deposition with the improvement of the probability-based deposition and resuspension boundary rather than the pure sorption boundary. The model is validated by the good agreement between the simulated and measured net sediment deposition. From the comparison of the probability-based boundary and pure the sorption boundary, the present model is much accurate for simulating the real particle motion near the channel bed, which suggests an improvement in the RDM.
- (4) In the present model, the deposition probability is used to illustrate the sediment motion at the leading edge of the vegetation patch, while both the resuspension and the deposition are rationally considered beyond the adjustment region. This study demonstrates that the main effect of the vegetation on the sediment transport varies at the different regions of the vegetation patch, which helps to investigate the underlying physical mechanism of the sediment transport near the channel bed.

Conflict of Interest

There are no real or perceived financial conflicts of interests for any author, no other affiliations for any author that may be perceived as having a conflict of interest with respect to the results of this paper.

Data Availability Statement

All the data used in this study have been reported elsewhere (Zhang et al., 2020; Zong & Nepf, 2010), and the data used to plot Figures 8 and 9 are available at Zenodo via <https://doi.org/10.5281/zenodo.5178754>.

Acknowledgments

The study reported here is financially supported by the Natural Science Foundation of China (Nos. 52020105006 and 11872285), the UK Royal Society – International Exchanges Program (IES\ R2\181122), and the Open Funding of State Key Laboratory of Water Resources and Hydropower Engineering Science (WRHES), Wuhan University (Project No. 2018HLG01).

References

- Abt, S., Clary, W. P., & Thornton, C. (1994). Sediment deposition and entrapment in vegetated streambeds. *Journal of Irrigation and Drainage Engineering*, 120(6), 1098–1111. [https://doi.org/10.1061/\(ASCE\)0733-9437\(1994\)120:6\(1098\)](https://doi.org/10.1061/(ASCE)0733-9437(1994)120:6(1098))
- Ai, Y. D., Liu, M., & Huai, W. X. (2020). Numerical investigation of flow with floating vegetation island. *Journal of Hydrodynamics*, 32(1), 31–43. <https://doi.org/10.1007/s42241-020-0004-6>
- Beheshti, A. A., & Ataie-Ashtiani, B. (2008). Analysis of threshold and incipient conditions for sediment movement. *Coastal Engineering*, 55(5), 423–430. <https://doi.org/10.1016/j.coastaleng.2008.01.003>
- Beuselinck, L., Steegen, A., Govers, G., Nachtergaele, J., Takken, I., & Poesen, J. (2000). Characteristics of sediment deposits formed by intense rainfall events in small catchments in the Belgian Loam Belt. *Geomorphology*, 32(1), 69–82. [https://doi.org/10.1016/S0169-555X\(99\)00068-9](https://doi.org/10.1016/S0169-555X(99)00068-9)
- Bohrer, G., Katul, G. G., Nathan, R., Walko, R. L., & Avissar, R. (2008). Effects of canopy heterogeneity, seed abscission and inertia on wind-driven dispersal kernels of tree seeds. *Journal of Ecology*, 96(4), 569–580. <https://doi.org/10.1111/j.1365-2745.2008.01368.x>
- Chen, Z., Jiang, C., & Nepf, H. M. (2013). Flow adjustment at the leading edge of a submerged aquatic canopy. *Water Resources Research*, 49(9), 5537–5551. <https://doi.org/10.1002/wrcr.20403>
- Cheng, N. S. (1997). A simplified settling velocity formula for sediment particle. *Journal of Hydraulic Engineering*, 123(2), 149–152. [https://doi.org/10.1061/\(ASCE\)0733-9429\(1997\)123:2\(149\)](https://doi.org/10.1061/(ASCE)0733-9429(1997)123:2(149))
- Choi, S., & Kwak, S. (2001). Theoretical and probabilistic analyses of incipient motion of sediment particles. *KSCE Journal of Civil Engineering*, 5(1), 59–65. <https://doi.org/10.1007/BF02830727>
- Diplas, P., Dancy, C. L., Celik, A. O., Valyrakis, M., Greer, K., & Tanju, A. (2008). The role of impulse on the initiation of particle movement under turbulent flow conditions. *Science*, 322(5902), 717–720. <https://doi.org/10.1126/science.1158954>
- Dou, G. R. (1960). On velocity of incipient motion. *Journal of Hydraulic Engineering*, 2(4), 46–62. (in Chinese).
- Duman, T., Trakhtenbrot, A., Poggi, D., Cassiani, M., & Katul, G. G. (2016). Dissipation intermittency increases long-distance dispersal of heavy particles in the canopy sublayer. *Boundary-Layer Meteorology*, 159(1), 41–68. <https://doi.org/10.1007/s10546-015-0112-y>
- Engelund, F., & Fredsoe, J. (1976). A sediment transport model for straight alluvial channels. *Nordic Hydrology*, 7(5), 293–306. <https://doi.org/10.2166/nh.1976.0019>
- Follett, E., Chamecki, M., & Nepf, H. M. (2016). Evaluation of a random displacement model for predicting particle escape from canopies using a simple eddy diffusivity model. *Agricultural and Forest Meteorology*, 224, 40–48. <https://doi.org/10.1016/j.agrformet.2016.04.004>
- Follett, E., Hays, C. G., & Nepf, H. M. (2019). Canopy-mediated hydrodynamics contributes to greater allelic richness in seeds produced higher in meadows of the coastal eelgrass *Zostera marina*. *Frontiers in Marine Science*, 6, 8. <https://doi.org/10.3389/fmars.2019.00008>
- Follett, E., & Nepf, H. M. (2012). Sediment patterns near a model patch of reedy emergent vegetation. *Geomorphology*, 179, 141–151. <https://doi.org/10.1016/j.geomorph.2012.08.006>
- Follett, E., & Nepf, H. M. (2018). Particle retention in a submerged meadow and its variation near the leading edge. *Estuaries and Coasts*, 41(3), 724–733. <https://doi.org/10.1007/s12237-017-0305-3>
- Fonseca, M. S., Ziemann, J. C., Thayer, G. W., & Fisher, J. S. (1983). The role of current velocity in structuring eelgrass meadows. *Estuarine, Coastal and Shelf Science*, 17, 367–380. [https://doi.org/10.1016/0272-7714\(83\)90123-3](https://doi.org/10.1016/0272-7714(83)90123-3)
- Gacia, E., Duarte, C. M., Marbà, N., Terrados, J., Kennedy, H., Fortes, M. D., & Tri, N. H. (2003). Sediment deposition and production in SE-Asia seagrass meadows. *Estuarine, Coastal and Shelf Science*, 56(5–6), 909–919. [https://doi.org/10.1016/S0272-7714\(02\)00286-X](https://doi.org/10.1016/S0272-7714(02)00286-X)
- Ganthy, F., Soissons, L., Sauriau, P., Verney, R., & Sottolichio, A. (2015). Effects of short flexible seagrass *Zostera noltei* on flow, erosion and deposition processes determined using flume experiments. *Sedimentology*, 62(4), 997–1023. <https://doi.org/10.1111/sed.12170>
- Ghisalberti, M. (2002). Mixing layers and coherent structures in vegetated aquatic flows. *Journal of Geophysical Research*, 107(C2). <https://doi.org/10.1029/2001JC000871>
- Ghisalberti, M., & Nepf, H. M. (2004). The limited growth of vegetated shear layers. *Water Resources Research*, 40(7). <https://doi.org/10.1029/2003WR002776>
- Ghisalberti, M., & Nepf, H. M. (2005). Mass transport in vegetated shear flows. *Environmental Fluid Mechanics*, 5, 527–551. <https://doi.org/10.1007/s10652-005-0419-1>
- Guo, Y. (2020). Empirical model for shields diagram and its applications. *Journal of Hydraulic Engineering*, 146(6), 4020038. [https://doi.org/10.1061/\(ASCE\)HY.1943-7900.0001739](https://doi.org/10.1061/(ASCE)HY.1943-7900.0001739)
- Houssais, M., Ortiz, C. P., Durian, D. J., & Jerolmack, D. J. (2015). Onset of sediment transport is a continuous transition driven by fluid shear and granular creep. *Nature Communications*, 6(1). <https://doi.org/10.1038/ncomms7527>
- Huai, W. X., Cheng, Z., Han, J., Zhang, L.-X., & Zeng, Y.-H. (2009). Mathematical model for the flow with submerged and emerged rigid vegetation. *Journal of Hydrodynamics*, 21(5), 722–729. [https://doi.org/10.1016/S1001-6058\(08\)60205-X](https://doi.org/10.1016/S1001-6058(08)60205-X)
- Huai, W. X., Li, S. L., Katul, G. G., Liu, M., & Yang, Z. (2021). Flow dynamics and sediment transport in vegetated rivers: A review. *Journal of Hydrodynamics*, 33(3), 400–420. <https://doi.org/10.1007/s42241-021-0043-7>
- Huai, W. X., Yang, L., & Guo, Y. K. (2020). Analytical solution of suspended sediment concentration profile: Relevance of dispersive flow term in vegetated channels. *Water Resources Research*, 56(7). <https://doi.org/10.1029/2019WR027012>
- Huai, W. X., Yang, L., Wang, W., Guo, Y. K., Wang, T., & Cheng, Y. (2019). Predicting the vertical low suspended sediment concentration in vegetated flow using a random displacement model. *Journal of Hydrology*, 578, 124101. <https://doi.org/10.1016/j.jhydrol.2019.124101>
- Huai, W. X., Zhang, J., Katul, G. G., Cheng, Y., Tang, X., & Wang, W. (2019). The structure of turbulent flow through submerged flexible vegetation. *Journal of Hydrodynamics*, 31(2), 274–292. <https://doi.org/10.1007/s42241-019-0023-3>
- Kim, H. S., Kimura, I., & Park, M. (2018). Numerical simulation of flow and suspended sediment deposition within and around a circular patch of vegetation on a rigid bed. *Water Resources Research*, 54(10), 7231–7251. <https://doi.org/10.1029/2017WR021087>
- Lawson, S. E., McGlathery, K. J., & Wiberg, P. L. (2012). Enhancement of sediment suspension and nutrient flux by benthic macrophytes at low biomass. *Marine Ecology Progress Series*, 448, 259–270. <https://doi.org/10.3354/meps09579>

- Liu, X. Y., Huai, W. X., Wang, Y., Yang, Z. H., & Zhang, J. (2018). Evaluation of a random displacement model for predicting longitudinal dispersion in flow through suspended canopies. *Ecological Engineering*, 116, 133–142. <https://doi.org/10.1016/j.ecoleng.2018.03.004>
- Marion, A., & Tregnaghi, M. (2013). A new theoretical framework to model incipient motion of sediment grains and implications for the use of modern experimental techniques. *Experimental and computational solutions of hydraulic problems*. Berlin Heidelberg: Springer. https://doi.org/10.1007/978-3-642-30209-1_5
- Nelson, J. M., Shreve, R. L., McLean, S. R., & Drake, T. G. (1995). Role of near-bed turbulence structure in bed load transport. *Water Resources Research*, 31(8), 2071–2086. <https://doi.org/10.1029/95WR00976>
- Nepf, H. M. (2012). Flow and transport in regions with aquatic vegetation. *Annual Review of Fluid Mechanics*, 44(1), 123–142. <https://doi.org/10.1146/annurev-fluid-120710-101048>
- Nepf, H. M., Ghisalberti, M., Murphy, E., & Murphy, E. (2007). Retention time and dispersion associated with submerged aquatic canopies. *Water Resources Research*, 43(4), 436–451. <https://doi.org/10.1029/2006WR005362>
- Nezu, I., & Nakagawa, H. (1993). *Turbulence in open channel flows*. Rotterdam: IAHR Monograph.
- Okamoto, T., Nezu, I., & Ikeda, H. (2012). Vertical mass and momentum transport in open-channel flows with submerged vegetations. *Journal of Hydro-environment Research*, 6(4), 287–297. <https://doi.org/10.1016/j.jher.2012.03.002>
- Raupach, M. R., Finnigan, J. J., & Brunei, Y. (1996). Coherent eddies and turbulence in vegetation canopies: The mixing-layer analogy. *Boundary-Layer Meteorology*, 78(3–4), 351–382. <https://doi.org/10.1007/bf00120941>
- Recking, A. (2009). Theoretical development on the effects of changing flow hydraulics on incipient bed load motion. *Water Resources Research*, 45(4). <https://doi.org/10.1029/2008WR006826>
- Stapleton, K., & Huntley, D. A. (1995). Seabed stress determinations using the inertial dissipation method and the turbulent kinetic energy method. *Earth Surface Processes and Landforms*, 20(9), 807–815. <https://doi.org/10.1002/esp.3290200906>
- Tang, C., Lei, J., & Nepf, H. M. (2019). Impact of vegetation-generated turbulence on the critical, near-bed, wave-velocity for sediment resuspension. *Water Resources Research*, 55(7), 5904–5917. <https://doi.org/10.1029/2018WR024335>
- Tanino, Y., & Nepf, H. M. (2008). Lateral dispersion in random cylinder arrays at high Reynolds number. *Journal of Fluid Mechanics*, 600, 339–371. <https://doi.org/10.1017/S0022112008000505>
- Taylor, G. I. (1921). Diffusion by continuous movements. *Proceedings of the London Mathematical Society*, 20(2), 196–212. <https://doi.org/10.1112/plms/s2-20.1.196>
- Tinoco, R. O., & Coco, G. (2016). A laboratory study on sediment resuspension within arrays of rigid cylinders. *Advances in Water Resources*, 92, 1–9. <https://doi.org/10.1016/j.advwatres.2016.04.003>
- Tinoco, R. O., & Coco, G. (2018). Turbulence as the main driver of resuspension in oscillatory flow through vegetation. *Journal of Geophysical Research: Earth Surface*, 123(5), 891–904. <https://doi.org/10.1002/2017JF004504>
- Tsujimoto, T. (1999). Fluvial processes in streams with vegetation. *Journal of Hydraulic Research*, 37(6), 789–803. <https://doi.org/10.1080/00221689909498512>
- Wang, Y. F., & Huai, W. X. (2019). Random walk particle tracking simulation on scalar diffusion with irreversible first-order absorption boundaries. *Environmental Science and Pollution Research*, 26, 33621–33630. <https://doi.org/10.1007/s11356-019-06422-1>
- Wilson, J. D. (2000). Trajectory models for heavy particles in atmospheric turbulence: Comparison with observations. *Journal of Applied Meteorology*, 39(11), 1894–1912. [https://doi.org/10.1175/1520-0450\(2000\)039<1894:TMFHPI>2.0.CO;2](https://doi.org/10.1175/1520-0450(2000)039<1894:TMFHPI>2.0.CO;2)
- Yager, E. M., & Schmeeckle, M. W. (2013). The influence of vegetation on turbulence and bed load transport. *Journal of Geophysical Research: Earth Surface*, 118(3), 1585–1601. <https://doi.org/10.1002/jgrf.20085>
- Yang, J. Q., Chung, H., & Nepf, H. M. (2016). The onset of sediment transport in vegetated channels predicted by turbulent kinetic energy. *Geophysical Research Letters*, 43(21), 11211–261268. <https://doi.org/10.1002/2016GL071092>
- Yang, J. Q., & Nepf, H. M. (2018). A turbulence-based bed-load transport model for bare and vegetated channels. *Geophysical Research Letters*, 45(19), 10410–428436. <https://doi.org/10.1029/2018GL079319>
- Yang, J. Q., & Nepf, H. M. (2019). Impact of vegetation on bed load transport rate and bedform characteristics. *Water Resources Research*, 55(7), 6109–6124. <https://doi.org/10.1029/2018WR024404>
- Zhang, J., Lei, J., Huai, W., & Nepf, H. M. (2020). Turbulence and particle deposition under steady flow along a submerged seagrass meadow. *Journal of Geophysical Research: Oceans*, 125(5). <https://doi.org/10.1029/2019JC015985>
- Zong, L., & Nepf, H. M. (2010). Flow and deposition in and around a finite patch of vegetation. *Geomorphology*, 116(3–4), 363–372. <https://doi.org/10.1016/j.geomorph.2009.11.020>